Impacts of Vegetation-generated Turbulence on Hyporheic Exchange

Qingjun Judy Yang[1] and Shih-Hsun Huang[2]

[1]University of Minnesota
[2]National Taiwan University

November 23, 2022

Abstract

Hyporheic exchange, or the exchange of water and solutes between surface and subsurface water at the sediment-water interface, regulates water quality and biogeochemical cycles in aquatic ecosystems. Vegetation, which is ubiquitous in aquatic ecosystems, is known to impact hyporheic exchange, yet how vegetation impacts hyporheic exchange remains to be characterized. Here, we show that at the same spatially and temporally averaged flow velocity U, vegetation-generated turbulence increases the rate of hyporheic exchange by a factor of four. By tracking the movement of fluorescent dye in a flume with index-matched sediment and translucent vegetation dowels, we demonstrate that turbulence-induced hyporheic exchange at the sediment-water interface can be characterized by a one-dimensional diffusion coefficient, D_{SWI}. We further demonstrate that D_{SWI} correlates with the total near-bed turbulent kinetic energy k_t rather than mean flow velocity U. A k_t-based model was developed to characterize the impacts of vegetation-generated turbulence on hyporheic exchange.

Impacts of Vegetation-generated Turbulence on Hyporheic Exchange

S. Huang[1,2], and J. Q. Yang[1,2]

[1] Saint Anthony Falls Laboratory, University of Minnesota, Minneapolis, MN 55414.

[2] Department of Civil, Environmental, and Geo-Engineering, University of Minnesota, Minneapolis, MN 55455.

Corresponding author: J. Q. Yang (judyyang@umn.edu)

Key Points:

- Vegetation-generated turbulence increases the exchange of solutes between surface and subsurface water in the hyporheic zone.
- Turbulence-induced hyporheic exchange can be characterized by a one-dimensional effective diffusion coefficient.
- The effective diffusion coefficient of turbulence-induced hyporheic exchange scales as total near-bed turbulent kinetic energy.

Abstract

Hyporheic exchange, or the exchange of water and solutes between surface and subsurface water at the sediment-water interface, regulates water quality and biogeochemical cycles in aquatic ecosystems. Vegetation, which is ubiquitous in aquatic ecosystems, is known to impact hyporheic exchange, yet how vegetation impacts hyporheic exchange remains to be characterized. Here, we show that at the same spatially and temporally averaged flow velocity U, vegetation-generated turbulence increases the rate of hyporheic exchange by a factor of four. By tracking the movement of fluorescent dye in a flume with index-matched sediment and translucent vegetation dowels, we demonstrate that turbulence-induced hyporheic exchange at the sediment-water interface can be characterized by a one-dimensional diffusion coefficient, D_{SWI}. We further demonstrate that D_{SWI} correlates with the total near-bed turbulent kinetic energy k_t rather than mean flow velocity U. A k_t-based model was developed to characterize the impacts of vegetation-generated turbulence on hyporheic exchange.

Plain Language Summary

The exchange of contaminants and nutrients between surface- and subsurface-water, in the hyporheic zone or sediment-water interface, controls the safety of our drinking water, as well as the metabolism of benthic microbes and the associated biogeochemical cycles. Vegetation, which is ubiquitous in aquatic ecosystems, has been found to affect the surface- and subsurface-exchange in the hyporheic zone and as such impact water quality and stream biogeochemical cycles. However, how vegetation impacts this exchange remains unclear, making it difficult to predict the spread of contaminants and biogeochemical cycles in streams, lakes, and coastal areas with vegetation. In this study, we directly visualized the release of fluorescent dye from transparent sediment into the surface water in a water-recirculating tank filled with translucent vegetation. We discovered that vegetation-generated turbulence can significantly increase the exchange in the hyporheic zone. Furthermore, we developed a semi-empirical equation that predict hyporheic exchange due to vegetation-generated turbulence. We believe this equation will help improve predictions of contaminant transport and biogeochemical cycles in streams and other aquatic ecosystems. The results of this study will also help ecologists design stream restoration projects that use vegetation to increase the retention and degradation of contaminants in sediment.

1 Introduction

Hyporheic zone refers to the region of sediment bed between surface stream and groundwater, where water, nutrients, and contaminants are consistently being exchanged (Boano et al., 2014; Boulton et al., 1998). The exchange between surface and subsurface water supplies nutrients and oxygen to underground microbes and as such controls the biogeochemical cycles and biodiversity and stability of stream bed (Battin et al., 2008; Jones Jr & Holmes, 1996; Tonina & Buffington, 2009; Wohl, 2016). The exchange in hyporheic zone also determines the retention and degradation of contaminants in stream, which controls the safety and quality of our recreation and drinking water (Grant et al., 2014; Lewandowski et al., 2011; McCallum et al., 2020). Fundamental understanding of the exchange in hyporheic zone is critical to predicting the biogeochemical cycles, biodiversity, and fate of contaminants in streams, yet such understanding is currently incomplete due to the complex multiscale characteristics of hyporheic exchange (Boano et al., 2014; Böhlke et al., 2009; Li et al., 2017; Stonedahl et al., 2012).

The exchange in hyporheic zone occurs over a wide range of spatial scales, from pore- to channel-scale (Boano et al., 2014; Li et al., 2017). First, at the pore-scale, turbulence generated by the surface flow can penetrate the top layers of the sediment bed, enhancing the mixing between surface and subsurface water (Buffington & Tonina, 2009; Clark et al., 2019; Li et al., 2017; Roche et al., 2018; Roche et al., 2019). Second, meso-scale in-channel structures such as bedforms, log jams, and in-channel vegetation induce a spatial gradient in hydraulic head at the sediment-water interface, which drives a bidirectional flow between surface and subsurface, i.e., water first enters the sediment and then back to the surface stream (Drummond et al., 2018; Dudunake et al., 2020; Marion et al., 2002; Tonina & Buffington, 2007; Wilhelmsen et al., 2021). Third, channel geometries such as meanderings generate a reach-scale hydraulic head gradient, creating bidirectional flows at the reach scale (Boano et al., 2006; Buffington & Tonina, 2009; Cardenas, 2009). Currently, extensive studies have been conducted to characterize the impacts of bedforms and channel geometries on hyporheic exchange (Boano et al., 2014; Marion et al., 2002; Packman et al., 2000; Salehin et al., 2004; Tonina & Buffington, 2007). However, other important drivers of hyporheic exchange have not been quantitatively characterized, particularly near-bed turbulence and in-channel vegetation (Kim & Kang, 2020; Roche et al., 2018; Roche et al., 2019; Voermans et al., 2017).

In this paper, we characterize the impacts of vegetation-generated turbulence on hyporheic exchange. We hypothesize that vegetation-generated turbulence can penetrate the sediment bed and increase the exchange between surface and subsurface water in the hyporheic zone. We propose using a one-dimensional (1D) effective diffusion coefficient, D_{SWI}, to characterize the turbulence-induced hyporheic exchange at the sediment-water interface (SWI). In addition, we hypothesize that D_{SWI} scales as the total near-bed turbulent kinetic energy k_t. Furthermore, we verify the 1D diffusion model and the scaling of D_{SWI} with k_t by conducting dye-visualization experiments in a water-recirculating flume filled with transparent hydrogel beads that simulate gravel bed and acrylic cylinders that simulate vegetation dowels.

2 Theories

2.1 1D diffusion model for hyporheic exchange at the sediment-water interface

Many studies show that near-bed turbulence in the surface water can penetrate the sediment grains, increasing the mixing between surface and subsurface water (Clark et al., 2019; Li et al., 2017; Packman et al., 2004; Roche et al., 2018; Roche et al., 2019). The turbulence-induced hyporheic exchange has been approximated as a vertical 1D diffusion process in channels with gravel beds (I. D. Chandler et al., 2016; Nagaoka & Ohgaki, 1990; Packman et al., 2004). Here we hypothesize that the turbulence-induced hyporheic exchange in vegetated channels with gravel flat beds is dominated by the vertical 1D diffusion process, which we further hypothesize can be characterized by a mixing coefficient D_{SWI}. Note that here we focus on the vertical hyporheic exchange across the sediment-water interface between the surface water and the top sediment layers. The variation in diffusivity with depth within the sediment as discussed in (I. Chandler et al., 2016) and the longitudinal dispersion (Bottacin-Busolin, 2017) are not the considered. Below we show an example of how we use D_{SWI} and a 1D diffusion model to predict the release of solutes from the pore water of the top sediment layers to the surface water in a water recirculating flume. In section 3, we describe how we use flume experiments to validate the 1D diffusion model.

First, at the beginning of the experiment, a solute is uniformly distributed in the pore space of the top several layers of grains of the sediment bed with concentration C_s and volume V_s. Due to turbulence-induced hyporheic mixing, the solute in the top sediment bed diffuses into the surface water, such that C_s decreases with time t. Once solute is diffused into the surface water, it gets quickly mixed in the recirculating flume with a uniform concentration C_w. For simplicity, we assume that the dye concentrations in the top sediment bed and in the surface water are both uniformly distributed, with volume V_s and V_w, respectively. We hypothesize that the exchange between surface and subsurface water at the sediment-water interface (SWI) can be characterized as a 1-D diffusion process with an effective hyporheic mixing coefficient D_{SWI} (m^2/s). Therefore, based on mass balance between the surface water and subsurface water:

$$\frac{dC_s}{dt} = -\frac{D_{SWI}}{\delta_D}\,\frac{A_{SWI}}{\phi_s V_s}(C_s - C_w) \tag{1}$$

$$\frac{dC_w}{dt} = -\frac{D_{SWI}}{\delta_D}\frac{A_{SWI}}{V_w}(C_w - C_s) \tag{2}$$

Here ϕ_s is the sediment porosity, A_{SWI} is the horizontal area of the sediment-water interface (m^2), and δ_D is the diffusion length scale (m, see Fig. S1 of the supplementary information document). For turbulence-induced hyporheic exchange, δ_D scales as the size of sediment diameter d. In this study, we set $\delta_D = d$ and use D_{SWI} to represent the effective hyporheic diffusion coefficient. Subtracting Eq. 1 by Eq. 2, we get

$$\frac{d(C_s - C_w)}{dt} = -\frac{D_{SWI}}{d}\frac{A_{SWI}}{\phi_s V_s V_w}\;(V_w - \phi_s V_s)(C_s - C_w) \tag{3}$$

Integrating Eq. 3 from time $t = 0$ s and assume the initial solute concentration in the surface water is zero, then

$$(C_s - C_w) = C_{s_0} e^{-k_h t} \tag{4}$$

where C_{s_0} is the initial dye concentration in the sediment bed and the decay coefficient $k_h = \frac{D_{SWI}}{d}\frac{A_{SWI}}{\phi_s V_s V_w}\;(V_w - \phi_s V_s)$. Based on the proposed 1D hyporheic diffusion model (Eq. 4), we anticipate that the concentration difference between the surface and subsurface water decays exponentially with time. The schematic diagram of the proposed 1D hyporheic diffusion model can be found in Fig. S1 of the supplementary information document.

2.2 Impacts of vegetation-generated turbulence on effective hyporheic diffusion coefficient

We further hypothesize that the effective hyporheic diffusion coefficient, D_{SWI}, scales as turbulent kinetic energy k_t because previous studies show that the rate of hyporheic mixing increases with turbulent kinetic energy (Kim & Kang, 2020). In the present study, we examine how D_{SWI} varies with the total near-bed k_t, under similar flow velocity U. Specifically, we compare D_{SWI} in channels without and with vegetation and examine whether and how D_{SWI} increases with vegetation-generated turbulence.

In bare or non-vegetated channels, the total near-bed k_t is contributed by the bed generated turbulence k_{tb}, which scales as mean flow velocity squared U^2 (Julien, 2010). In vegetated channel, vegetation generates additional turbulence k_{tv}, which is a function of flow velocity U and vegetation characteristics including vegetation frontal area per unit volume a and vegetation stem diameter d (Heidi M. Nepf, 2012; Tanino & Nepf, 2008; Yang et al., 2016). Previous studies show that the total near-bed turbulent kinetic energy in vegetated channels can be approximated as the sum of bed-generated k_{tb} and vegetation-generated k_{tv} (Yang et al., 2016; Yang & Nepf, 2018, 2019), namely,

$$k_t = k_{tb} + k_{tv}. \tag{5}$$

Therefore, at the same U, the total near-bed turbulent kinetic energy in the vegetated channel is larger than the total near-bed k_t in bare channels without vegetation. We anticipate that at the same U, the increase in total near-bed k_t due to vegetation will increase the effective hyporheic diffusion coefficient D_{SWI}. Furthermore, we hypothesize that D_{SWI} scales as the total near-bed k_t. In the following sections, we use flume experiments to examine this hypothesis.

3 Materials and Methods

3.1 Experimental set up

Hyporheic exchange experiments were conducted in a race-track flume at the University of Minnesota's St. Anthony Falls Laboratory. The flume is 14-m-long and 60-cm-wide and has a 60-cm-wide by 150-cm-long straight test section (Fig. 1). The water depth in all experiments was 20.0 ± 0.1 cm. The flow in the flume was driven by a propeller with cross-sectionally averaged flow velocity ranging between 0.7 to 15.4 cm/s.

The bottom of the test section was removed, and the space underneath (18-cm-deep) was filled with transparent hydrogel beads (5.6 ± 0.6 mm in diameter) to simulate a gravel bed. Method to make the hydrogel beads were developed by Ma et al. (2019) and described in the supplementary information document. To keep the hydrogel beads in place and the sediment bed flat, a black polyester mesh (4 mm pore size) was placed on top of the beads. Note that, during the experiments without vegetation, a small bed form with bedform height 1 cm was noticed. This may increase the near-bed turbulent kinetic energy. However, we anticipate that this small bed form will not affect our results, because we directly measured near-bed turbulent kinetic energy as described in the following paragraphs.

Translucent acrylic dowels with 6.4±0.1 mm diameter were inserted in a staggered pattern (Fig. S4) on a perforated PVC boards placed below the transparent soil. The solid volume fraction of vegetation in this study is 0.05, in the range of typical values found in marshes (Heidi M Nepf, 2012; Yang et al., 2016; Yang & Nepf, 2018). The vegetation fontal area per unit volume is 9.8 m^{-1} and the stem density is 1547 $\mathrm{stems/m^2}$.

Instantaneous flow velocity was measured using an Acoustic-Doppler Velocimeter (Nortek Vectrino, Norway) mounted on a 2-D moving system with 200 Hz sampling rate for 2.5 minutes. We tested that 2.5-minute duration is sufficient to obtain convergent mean flow velocity and turbulent kinetic energy. Solid glass beads with specific gravity 2.57 and mean diameter 35 micrometers (3000 E-Spheriglass; Potters Industries Inc., Pennsylvania) were added to the water as seeding particles. Measurements with SNR below 15 dB were removed from data analysis. A bivariate kernel density function was used to remove noise signals from velocity measurements (Islam & Zhu, 2013). Four vertical velocity profiles were measured to capture spatial heterogeneity in velocity measurements (Yang et al., 2016). We tested that four profiles are enough to obtain convergent spatially averaged mean flow velocity and turbulent kinetic energy profiles. For non-vegetated cases, the velocity profiles were measured at four horizontal locations 8-cm apart from each other. For vegetated cases, velocity measurements were taken between two rows of dowels.

The locations of the velocity measurements for the vegetated cases are shown in Fig. S4 of the supplementary information document.

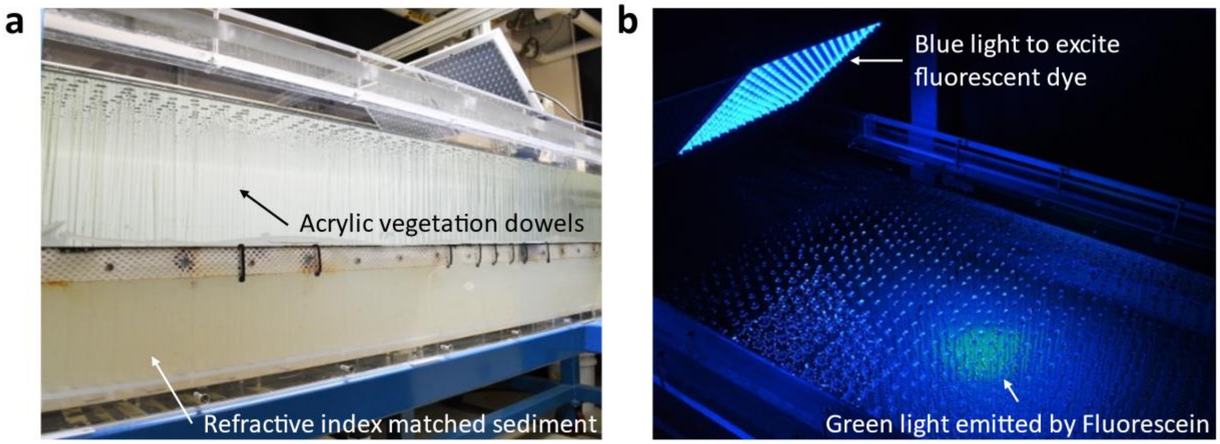

Figure 1. Experiments in a water recirculating flume to directly visualize the exchange of fluorescent dye between surface and subsurface water. Refractive-index-matched sediment and translucent vegetation dowels were used.

3.2 Fluorescent dye release experiments

Fluorescent dye was used as a tracer of the hyporheic exchange. The dye solution was prepared by adding fluorescein sodium salt (Sigma-Aldrich F6377) to DI water at 0.002‰ weight ratio. The dye, fluorescein sodium, emit green light at 520-nm wavelength, when excited by blue light at 490-nm wavelength (Osenbroch et al., 2005). One square lamp (30-cm-width by 30-cm-length) with blue LED arrays were placed at the center of the channel and 33 cm above the water surface. The angle between lamp and ground is 40°. The camera was placed 120 cm above the sediment bed. The light emitted from the dye was passed through a green light filter (FGV9S; Thorlabs, Newton) and captured by an industrial camera (BFS-U3-16S2C-CS; FLIR Systems, Wilsonville) with a 6 mm focal length lens (ArduCAM, China).

The fluorescent intensity of the fluorescein dye in the sediment were calibrated against the dye concentration in the sediment. First, we placed a box filled with beads and known concentrations of fluorescein dye under the mesh. Then, we illuminated the dye and hydrogel beads in the box with the blue LED lamp and measured the average intensity of the emitted green light using the downward-facing camera with a green light filter (as described in the above paragraph). Our measurements show that the emitted light intensity is linearly proportional to the accumulative dye concentration, or dye concentration times the depth of top sediment layers filled with dye. The calibration results are shown in Fig. S5 of the supplementary information document. The linear relationship indicates that the fluorescent intensity can be used to represent dye concentration in the sediment.

Fluorescent dye release experiments were conducted to verify the proposed 1D diffusion model (Eqs. 1-4) and investigate the impacts of turbulence on the effective hyporheic diffusion coefficient. First, 0.002‰ fluorescein dye were injected into a 44×43 cm^2 sediment area up to 5 cm deep (accumulative dye concentration $(1.286 \pm 0.006) \times 10^{-3}$ mg/cm^2) using a peristaltic pump (L/S 7550-50; Masterflex, Germany). Afterwards, flows were recirculated in the flume using a propeller. The decrease in the concentration of the dye in the sediment layer were captured by images taken every 5 minutes for a 16-hour duration using a downward facing camera. Experiments without and with vegetation were conducted at a range of flow velocities. The dye concentration in the sediment pore space was estimated by the intensity of pixels occupied by the pore space. Pixels occupied by vegetation and the mesh that hold sediment bed in place were removed (see the supplementary information document for the details of image processing).

Note that once dye leaves the sediment, it is quickly diluted in the surface water. Our experiments show that the dye in the surface water, whose concentration is much smaller than the dye concentration in the sediment, does not affect the results, i.e., the light emitted captured by the camera above the water surface is mainly contributed by the dye in the sediment.

4 Results

4.1 Dye release experiments verify the proposed 1D hyporheic diffusion model

First, we use dye release experiments described in section 3.2 to verify the proposed 1D hyporheic diffusion model (Eqs. 1-4). After fluorescent dye that emits green light was injected into the top sediment layer (5 cm), flow with controlled velocity was started at time t = 0 h. As the dye diffuses into the surface water, it is quickly diluted to a negligible concentration. The intensity of the emitted green light, which represents the dye concentration in the sediment (Fig. S5), was captured by a downward looking camera. The snapshots of the dye at different times show that the dye concentration in the sediment bed decreases over time (Fig. 2), consistent with the fact that the dye in the sediment diffuses into the surface water due to hyporheic exchange or diffusion at the sediment-water interface.

To capture the rate of dye diffusing into the surface water, the average intensity of the green light emitted by the fluorescent dye in the pore space was plotted over time. Fig. 3 shows two representative cases without and with vegetation at a similar spatially and temporally averaged flow velocity U. The decrease in dye concentrations in vegetated channels occurred much faster in a vegetated channel than in a bare channel, indicating that vegetation-generated turbulence indeed increased the diffusion or exchange of solute at the sediment-water interface. To capture the rate of diffusion, the measured average intensity of the fluorescent dye versus time was fitted to the proposed 1D hyporheic diffusion model (Eqs. 1-4), which is an exponential decay model with the decay coefficient determined by the effective hyporheic diffusion coefficient D_{SWI}. The curves in Fig. 3 show that dye concentration in the sediment indeed decays exponentially, indicating that our proposed 1D hyporheic diffusion model (Eqs. 1-4) can be used to characterize the turbulence-induced mixing at the sediment-water interface. At a similar flow velocity around 4 cm/s, the fitted effective hyporheic diffusion coefficient D_{SWI} for the case without vegetation is $1.9 \times 10^{-10}\,\mathrm{m}^2/s$, about four times smaller than the case with vegetation with $D_{SWI} = 7.3 \times 10^{-10}\,\mathrm{m}^2/s$, indicating that vegetation-generated turbulence can increase the rate of hyporheic diffusion by a factor of 4.

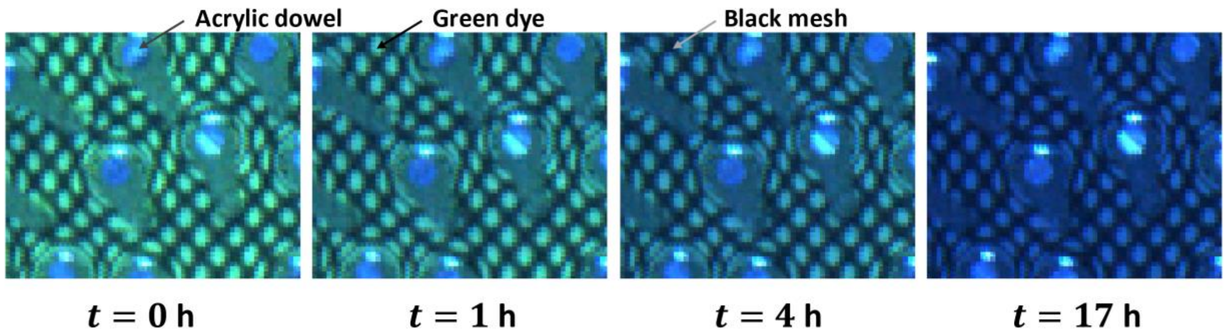

Figure 2. Images showing the decrease of the concentration of a fluorescent dye in the sediment over time during a dye release experiment. The dye fluorescein, illuminated by a blue light lamp, emitted green light. The intensity of the emitted green light scales with the accumulative dye concentration in the sediment (Fig. S5). Note that pixels occupied by the vegetation (the three rows of blue circles) and the black mesh were removed from images when the light intensity was calculated (see the supplementary information document for details). The vegetation volume fraction for this case is 0.05 and the mean flow velocity is 0.7 cm/s. Flow with controlled velocity was started at $t = 0$ h.

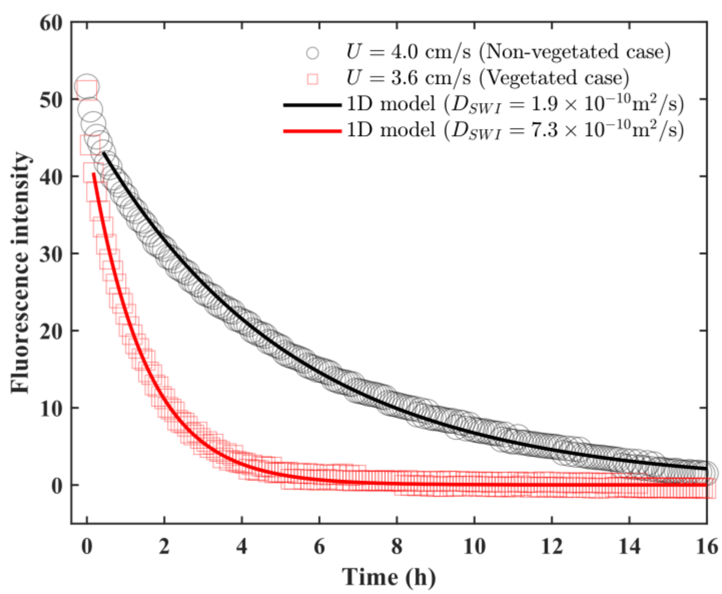

Figure 3. The concentration of the fluorescent dye in the sediment, represented by the intensity of the emitted fluorescent green light, decays exponentially over time, confirming the proposed 1D hyporheic diffusion model (Eqs. 1-4). The black and red symbols represent intensity measurements in channels without vegetation and with vegetation of volume fraction $\phi = 0.05$, respectively, at a similar flow velocity 4 cm/s. The black and red solid curves represent the fit of the measurements to the 1D diffusion model (Eq. 1). The fitted effective hyporheic diffusion coefficients, D_{SWI}, were 1.9×10^{-10} and 7.3×10^{-10} m^2/s for cases without vegetation (black) and with vegetation (red), respectively. The R^2 of the model fit for the non-vegetated and vegetated cases are 0.996 and 0.997, respectively.

4.2 The effective hyporheic diffusion coefficient scales with turbulent kinetic energy

To test our hypothesis that the hyporheic diffusion rate at the sediment-water interface is controlled by the total near-bed turbulent kinetic energy k_t, we calculated the effective hyporheic diffusion coefficient D_{SWI} for cases without vegetation and with vegetation of volume fraction $\phi = 0.05$ at different mean velocities U. For cases without vegetation, the total near-bed turbulent kinetic energy k_t equals the bed-generated turbulent kinetic energy, which scales with U^2. For cases with vegetation, at the same U, vegetation generates additional turbulence (Eq. 5) such that the total near-bed turbulent kinetic energy k_t is larger in vegetated channel than in non-vegetated channels. By comparing D_{SWI} versus U and k_t for cases without and with vegetation, we exam whether the diffusion rate at the sediment-water interface is controlled by mean flow velocity or turbulent kinetic energy. The calculated D_{SWI} were plotted against U and k_t for cases without vegetation and with vegetation in Fig. 4. As shown in the figure, for cases without and with vegetation, D_{SWI} increases with increasing U, consistent with the fact that flows increase diffusion or hyporheic exchange at the sediment-water interface. However, at the same U, vegetation generated turbulence increased effective hyporheic diffusion coefficient significantly, e.g., by about a factor of 4 at $U \approx 0.04$ m/s. Compared with the distinct D_{SWI} versus U curves for the non-vegetated and vegetated cases, the D_{SWI} versus k_t measurements agreed within uncertainty for both non-vegetated and vegetated cases, suggesting that the effective hyporheic diffusion coefficient at sediment-water interface is controlled by the total near-bed turbulence intensity k_t, confirming our hypothesis that the effective hyporheic diffusion coefficient at the sediment-water interface, D_{SWI}, scales with k_t.

Note that here the vegetation solid volume fraction $a > 4.3\ \mathrm{m}^{-1}$ such that the spatial variations in near-bed flow velocity, bed shear stress, and turbulent kinetic energy are insignificant (Stoesser et al., 2010; Yang et al., 2015) and as such the spatially averaged turbulent kinetic energy k_t can be used to predict D_{SWI}. We caution that for sparse vegetation with $a < 4.3\ \mathrm{m}^{-1}$, the spatial variation in near-bed turbulent kinetic energy may be significant, which could induce additional hyporheic exchange.

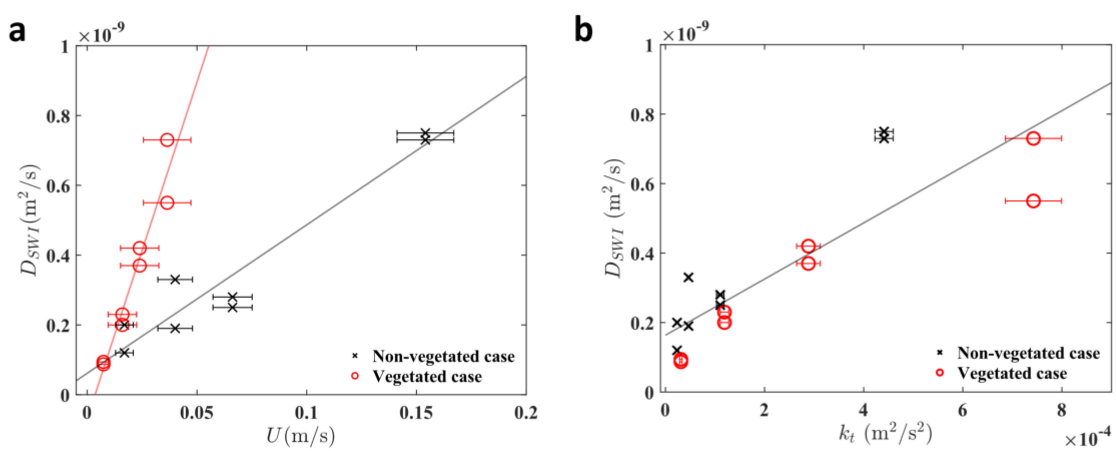

Figure 4. (a) The fitted hyporheic diffusion coefficient D_{SWI} versus mean flow velocity U for cases without vegetation (black) and with vegetation of volume fraction $\phi = 0.05$ (red). The black line ($y = (4.2x - 0.06) \times 10^{-7}$) and red line ($y = (1.9x - 0.007) \times 10^{-6}$) represent linear fits

to measurements without and with vegetation with $R^2 = 0.93$ and $R^2 = 0.94$, respectively. (b) The measured D_{SWI} versus measured total near-bed turbulent kinetic energy k_t for cases without vegetation (black) and with vegetation (red). The black line ($y = (8.1x - 0.002) \times 10^{-5}$) represents the linear fit to all the measurements with $R^2 = 0.76$. To reflect the spatial heterogeneity of velocity in the channel, U and k_t were calculated as the mean of velocity measured at 4 horizontal locations. U is the cross sectionally-averaged velocity; k_t is the horizontally-averaged turbulent kinetic energy measured at about 2 cm above the flume bed. The locations of measurements have been discussed in the Method section.

5 Conclusions

Turbulence has been recognized to enhance the exchange between surface and subsurface water in the hyporheic zone, yet the impacts of vegetation-generated turbulence on hyporheic exchange have not been characterized. Here we propose a 1D diffusion model to characterize the turbulence-induced hyporheic mixing in vegetated channels. By conducting tracer experiments using fluorescent dye and refractive-index-matched sediment, we show that the turbulence-induced hyporheic exchange at the sediment-water interface can be characterized by a 1D diffusion process with an effective hyporheic diffusion coefficient D_{SWI}. We demonstrate that at the same spatially and temporally averaged flow velocity U, vegetation generates additional near-bed turbulence and as such increases D_{SWI} by up to a factor of four when compared with channels without vegetation. We further demonstrate that D_{SWI} scales with the total near-bed turbulent kinetic energy k_t instead of U. The results of the proposed 1D hyporheic exchange model will enable quantitative analysis of the impacts of turbulence and vegetation, which are common in aquatic habitats, on the exchange of contaminants and nutrients in the hyporheic zone.

Acknowledgments

This study was supported by JQ Yang's startup funds and Minnesota Water Research Fund. The authors would like to thank Sam Nguyen for his assistance with the experiments, Peter Kang for insightful discussions, and Ben Erickson and Erik Steen for help with the flume.

Data Availability Statement

The raw data and results of the dye injection experiments conducted in this study have been deposited in The Data Repository for University of Minnesota (https://doi.org/10.13020/W282-JJ11).

The codes used to process the images and fit the washout curves has been deposited to Zenodo (https://doi.org/10.5281/zenodo.5755805).

References

Battin, T. J., Kaplan, L. A., Findlay, S., Hopkinson, C. S., Marti, E., Packman, A. I., . . . Sabater, F. (2008). Biophysical controls on organic carbon fluxes in fluvial networks. *Nature geoscience*, *1*(2), 95-100.

Boano, F., Camporeale, C., Revelli, R., & Ridolfi, L. (2006). Sinuosity-driven hyporheic exchange in meandering rivers. *Geophysical Research Letters*, *33*(18).

Boano, F., Harvey, J. W., Marion, A., Packman, A. I., Revelli, R., Ridolfi, L., & Wörman, A. (2014). Hyporheic flow and transport processes: Mechanisms, models, and biogeochemical implications. *Reviews of Geophysics*, *52*(4), 603-679.

Bottacin-Busolin, A. (2017). Non-Fickian dispersion in open-channel flow over a porous bed. *Water Resources Research*, *53*(8), 7426-7456.

Boulton, A. J., Findlay, S., Marmonier, P., Stanley, E. H., & Valett, H. M. (1998). The functional significance of the hyporheic zone in streams and rivers. *Annual review of Ecology and systematics*, *29*(1), 59-81.

Buffington, J. M., & Tonina, D. (2009). Hyporheic exchange in mountain rivers II: Effects of channel morphology on mechanics, scales, and rates of exchange. *Geography Compass*, *3*(3), 1038-1062.

Böhlke, J. K., Antweiler, R. C., Harvey, J. W., Laursen, A. E., Smith, L. K., Smith, R. L., & Voytek, M. A. (2009). Multi-scale measurements and modeling of denitrification in streams with varying flow and nitrate concentration in the upper Mississippi River basin, USA. *Biogeochemistry*, *93*(1), 117-141.

Cardenas, M. B. (2009). A model for lateral hyporheic flow based on valley slope and channel sinuosity. *Water Resources Research*, *45*(1).

Chandler, I., Guymer, I., Pearson, J., & Van Egmond, R. (2016). Vertical variation of mixing within porous sediment beds below turbulent flows. *Water resources research*, *52*(5), 3493-3509.

Chandler, I. D., Guymer, I., Pearson, J. M., & van Egmond, R. (2016). Vertical variation of mixing within porous sediment beds below turbulent flows. *Water resources research, 52*(5), 3493-3509. https://doi.org/10.1002/2015WR018274

Clark, J. J., Qian, Q., Voller, V. R., & Stefan, H. G. (2019). Hyporheic exchange in a gravel bed flume with and without traveling surface waves. *Advances in Water Resources*, *123*, 120-133.

Drummond, J. D., Larsen, L. G., González-Pinzón, R., Packman, A., & Harvey, J. W. (2018). Less fine particle retention in a restored versus unrestored urban stream: Balance between hyporheic exchange, resuspension, and immobilization. *Journal of Geophysical Research: Biogeosciences*, *123*(4), 1425-1439.

Dudunake, T., Tonina, D., Reeder, W., & Monsalve, A. (2020). Local and Reach-Scale Hyporheic Flow Response From Boulder-Induced Geomorphic Changes. *Water Resources Research*, *56*(10), e2020WR027719.

Grant, S. B., Stolzenbach, K., Azizian, M., Stewardson, M. J., Boano, F., & Bardini, L. (2014). First-order contaminant removal in the hyporheic zone of streams: Physical insights from a simple analytical model. *Environmental science & technology*, *48*(19), 11369-11378.

Huang, S.-H., & Yang, J. Q. (2021). *Experimental data of vegetation-induced hyporheic exchange experiment in Ecoflume of St. Anthony Falls Laboratory on 2021 (29GB)*. https://doi.org/https://doi.org/10.13020/W282-JJ11

Islam, M. R., & Zhu, D. Z. (2013). Kernel density–based algorithm for despiking ADV data. *Journal of Hydraulic Engineering*, *139*(7), 785-793.

Jones Jr, J. B., & Holmes, R. M. (1996). Surface-subsurface interactions in stream ecosystems. *Trends in Ecology & Evolution*, *11*(6), 239-242.

Julien, P. Y. (2010). *Erosion and sedimentation* (Second edition.. ed.). Cambridge : Cambridge University Press.

Kim, J. S., & Kang, P. K. (2020). Anomalous transport through free-flow-porous media interface: Pore-scale simulation and predictive modeling. *Advances in Water Resources*, *135*, 103467.

Lewandowski, J., Putschew, A., Schwesig, D., Neumann, C., & Radke, M. (2011). Fate of organic micropollutants in the hyporheic zone of a eutrophic lowland stream: Results of a preliminary field study. *Science of the Total Environment*, *409*(10), 1824-1835.

Li, A., Aubeneau, A. F., Bolster, D., Tank, J. L., & Packman, A. I. (2017). Covariation in patterns of turbulence-driven hyporheic flow and denitrification enhances reach-scale nitrogen removal. *Water Resources Research*, *53*(8), 6927-6944.

Ma, L., Shi, Y., Siemianowski, O., Yuan, B., Egner, T. K., Mirnezami, S. V., . . . Cademartiri, L. (2019). Hydrogel-based transparent soils for root phenotyping in vivo. *Proceedings of the National Academy of Sciences*, *116*(22), 11063-11068.

Marion, A., Bellinello, M., Guymer, I., & Packman, A. (2002). Effect of bed form geometry on the penetration of nonreactive solutes into a streambed. *Water Resources Research*, *38*(10), 27-21-27-12.

McCallum, J. L., Höhne, A., Schaper, J. L., Shanafield, M., Banks, E. W., Posselt, M., . . . Lewandowski, J. (2020). A numerical stream transport modeling approach including multiple conceptualizations of hyporheic exchange and spatial variability to assess contaminant removal. *Water Resources Research*, *56*(3), e2019WR024987.

Nagaoka, H., & Ohgaki, S. (1990). Mass transfer mechanism in a porous riverbed. *Water research (Oxford), 24*(4), 417-425. https://doi.org/10.1016/0043-1354(90)90223-S

Nepf, H. M. (2012). Flow and transport in regions with aquatic vegetation. *Annual review of fluid mechanics*, *44*, 123-142.

Nepf, H. M. (2012). Flow and Transport in Regions with Aquatic Vegetation. *Annual review of fluid mechanics*, *44*(1), 123-142. https://doi.org/10.1146/annurev-fluid-120710-101048

Osenbroch, L. K. H., Hjertager, B. H., & Solberg, T. (2005). Experiments and CFD modelling of fast chemical reaction in turbulent liquid flows. *International Journal of Chemical Reactor Engineering*, *3*(1).

Packman, A. I., Brooks, N. H., & Morgan, J. J. (2000). Kaolinite exchange between a stream and streambed: Laboratory experiments and validation of a colloid transport model. *Water Resources Research*, *36*(8), 2363-2372.

Packman, A. I., Salehin, M., & Zaramella, M. (2004). Hyporheic Exchange with Gravel Beds: Basic Hydrodynamic Interactions and Bedform-Induced Advective Flows. *Journal of hydraulic engineering (New York, N.Y.)*, *130*(7), 647-656. https://doi.org/10.1061/(ASCE)0733-9429(2004)130:7(647)

Roche, K., Blois, G., Best, J., Christensen, K., Aubeneau, A., & Packman, A. (2018). Turbulence links momentum and solute exchange in coarse-grained streambeds. *Water Resources Research*, *54*(5), 3225-3242.

Roche, K. R., Li, A., Bolster, D., Wagner, G. J., & Packman, A. I. (2019). Effects of turbulent hyporheic mixing on reach-scale transport. *Water Resources Research*, *55*(5), 3780-3795.

Salehin, M., Packman, A. I., & Paradis, M. (2004). Hyporheic exchange with heterogeneous streambeds: Laboratory experiments and modeling. *Water Resources Research*, *40*(11).

Stoesser, T., Kim, S., & Diplas, P. (2010). Turbulent flow through idealized emergent vegetation. *Journal of Hydraulic Engineering*, *136*(12), 1003-1017.

Stonedahl, S. H., Harvey, J. W., Detty, J., Aubeneau, A., & Packman, A. I. (2012). Physical controls and predictability of stream hyporheic flow evaluated with a multiscale model. *Water Resources Research*, *48*(10).

Tanino, Y., & Nepf, H. M. (2008). Lateral dispersion in random cylinder arrays at high Reynolds number. *Journal of fluid mechanics*, *600*, 339-371. https://doi.org/10.1017/S0022112008000505

Tonina, D., & Buffington, J. M. (2007). Hyporheic exchange in gravel bed rivers with pool-riffle morphology: Laboratory experiments and three-dimensional modeling. *Water Resources Research*, *43*(1).

Tonina, D., & Buffington, J. M. (2009). Hyporheic exchange in mountain rivers I: Mechanics and environmental effects. *Geography Compass*, *3*(3), 1063-1086.

Voermans, J., Ghisalberti, M., & Ivey, G. (2017). The variation of flow and turbulence across the sediment–water interface. *Journal of Fluid Mechanics*, *824*, 413-437.

Wilhelmsen, K., Sawyer, A., Marshall, A., McFadden, S., Singha, K., & Wohl, E. (2021). Laboratory Flume and Numerical Modeling Experiments show Log Jams and Branching Channels increase Hyporheic Exchange. *Water Resources Research*, *57*(9), e2021WR030299.

Wohl, E. (2016). Spatial heterogeneity as a component of river geomorphic complexity. *Progress in Physical Geography*, *40*(4), 598-615.

Yang, J., Chung, H., & Nepf, H. (2016). The onset of sediment transport in vegetated channels predicted by turbulent kinetic energy. *Geophysical Research Letters*, *43*(21), 11,261-211,268.

Yang, J. Q., Kerger, F., & Nepf, H. M. (2015). Estimation of the bed shear stress in vegetated and bare channels with smooth beds: ESTIMATION OF THE BED SHEAR STRESS. *Water resources research*, *51*(5), 3647-3663. https://doi.org/10.1002/2014WR016042

Yang, J. Q., & Nepf, H. M. (2018). A turbulence-based bed-load transport model for bare and vegetated channels. *Geophysical Research Letters*, *45*(19), 10,428-410,436.

Yang, J. Q., & Nepf, H. M. (2019). Impact of vegetation on bed load transport rate and bedform characteristics. *Water Resources Research*, *55*(7), 6109-6124.

Geophysical Research Letters

Supporting Information for

Impacts of Vegetation-generated Turbulence on Hyporheic Exchange

S. Huang[1,2], and J. Q. Yang[1,2]

[1] Saint Anthony Falls Laboratory, University of Minnesota, Minneapolis, MN 55414.

[2] Department of Civil, Environmental, and Geo-Engineering, University of Minnesota, Minneapolis, MN 55455.

Contents of this file

Introduction

This supporting information contains Text S1-2 and Figures S1-6. In Text S1, the procedure to make hydrogel beads used in the experiments is briefly summarized. Image processing steps that were used to generate the washout curves and the fitting process of the 1D diffusion model are described in Text S2. Fig. S1 shows the schematic diagram of the 1-D hyporheic diffusion model. Figs. S2 and S3 are images related to production of hydrogel beads. Fig. S4 shows the location of velocity measurements in vegetated channels. Fig. S5 shows the results of dye calibration. Fig. S6 describes the imaging processing steps.

Text S1.

The hydrogel beads were made following the procedure proposed by Ma et al. (2019). First, sodium alginate (Sigma-Aldrich W201502) and Gellan Gum (Sigma-Aldrich P8169) were mixed with deionized water, and their final concentrations were 0.24 wt% and 0.96 wt%, respectively. To make sodium alginate and Gellan Gum fully dissolve into the water, the gel solution was autoclaved with the liquids cycle (sterilization temperature: 121 ℃, sterilize time: 30 minutes). After cooling down overnight, the polymer solution was dropped into 10 mM magnesium chloride solution ($MgCl_2$, Millipore 442611-M) through plastic tubes (4 mm I.D.), as shown in Fig. S2. The magnesium ions cause sodium alginate and Gellan Gum to cross link and form discrete spheroid hydrogel beads (Fig. S3). The diameters of resulting hydrogel beads are 5.6±0.6 mm.

Text S2.

Here we describe the imaging processing steps to calculate the dye intensity in the sediment from images shown in Fig. 2. First, the recorded images were cropped to contain several repeated areas of vegetation dowels, and the area occupied by and near plastic dowels was removed. Second, the histogram of intensity of remaining pixels was fitted by the sum of two normalized histograms (Fig. S6). Based on the histograms, the pixels were classified into two categories: (i) pixels occupied by the mesh were identified as the pixels with intensity histogram following the distribution with lower mean intensity and (ii) pixels occupied by hydrogel beads and pore water were identified by as pixels with intensity histogram following the distribution with higher mean intensity. Note that for consistency, the number of pixels belong to the two histograms were kept at 59:41 ratio. Third, fluorescent intensity of the sediment was estimated as the average of the intensity of pixels occupied by the hydrogel beads and pore water. This fluorescent intensity was used to represent the average dye intensity in the dye concertation versus time curves, or washout curves, shown in Fig 3.

After we obtained the dye concentration versus time curves, we fitted the curves to the 1D diffusion model (Eqs. 1-4). The background image intensity (the image intensity without dye) and the effective hyporheic diffusion coefficient D_{SWI} were chosen as fitting parameters. First, the model was solved numerically, and the root mean square error between the modeled washout curve and the experimental washout curve was calculated by linear interpolating the modeled washout curve at the collection time of each data point in the experiment. Both background image intensity and D_{SWI} were adjust in each iteration to find the minimum root mean square error. The code of the fitting process can be found on the GitHub (https://github.com/Shih-HsunHuang/Vegetated-induced-hyporheic-exchange).

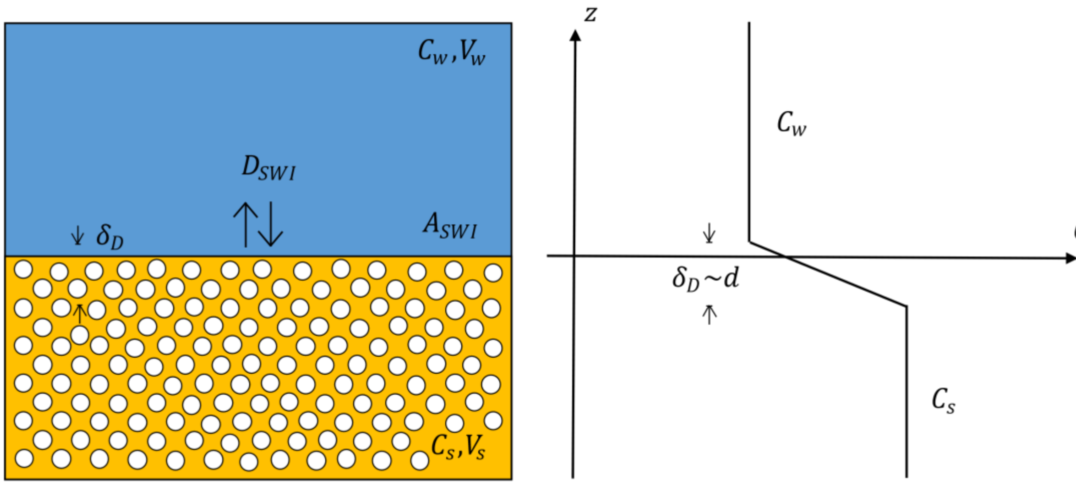

Figure S1. Schematic diagram of the 1-D hyporheic diffusion model. The blue and yellow area indicate the surface water and sediment bed, respectively. $\boldsymbol{C}$ denotes the concentration of a solute in surface water and pore water within the sediment.

Figure S2. The dropping system to make hydrogel beads with controlled size. The polymer solution was poured into the cups and dropped into the 10 mM magnesium chloride solution in the container blow the cups due to gravity.

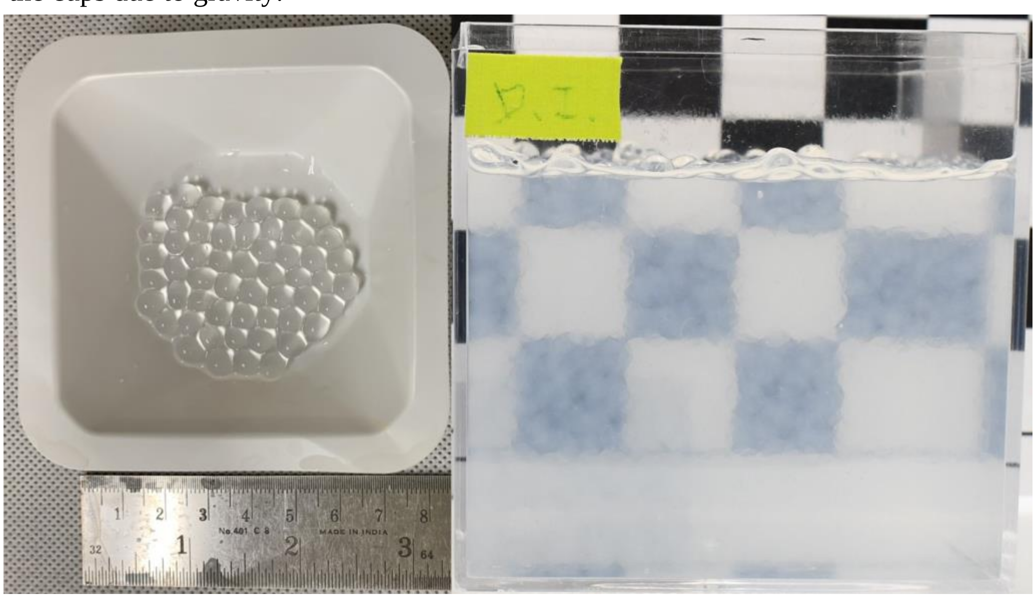

Figure S3. The hydrogel beads. The width of the container with hydrogel beads in water on the right image is 8cm.

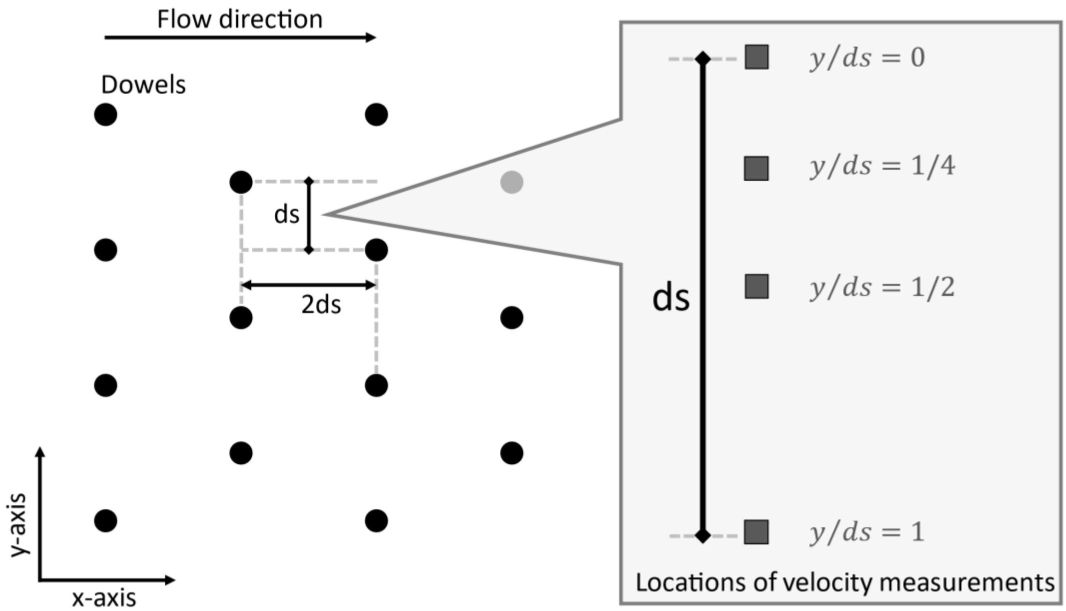

Figure S4. The locations of the velocity measurements for the vegetated cases (the square symbols). The flow direction is long the $\boldsymbol{x}$-axis, i.e., from the left to the right. The black circles represent vegetation dowels.

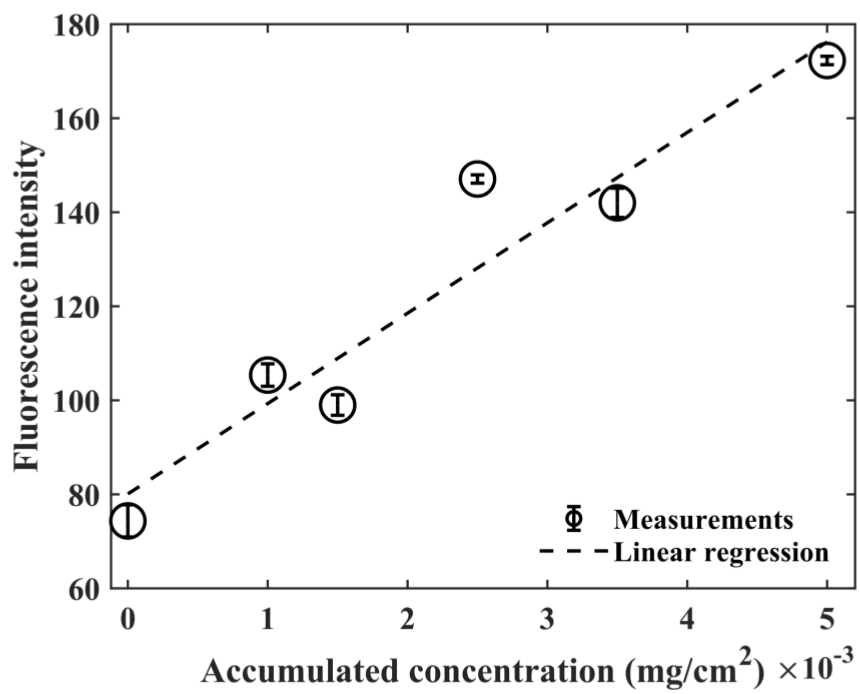

Figure S5. The measured average intensity of the green light emitted from the fluorescein dye in the top sediment layer is calibrated against the accumulated dye concentration, which is the dye concentration times the depth of sediment layers filled with dye. The dashed line represents the linear fit $\boldsymbol{y = 19224x + 80}$ with $\boldsymbol{R^2 = 0.91}$.

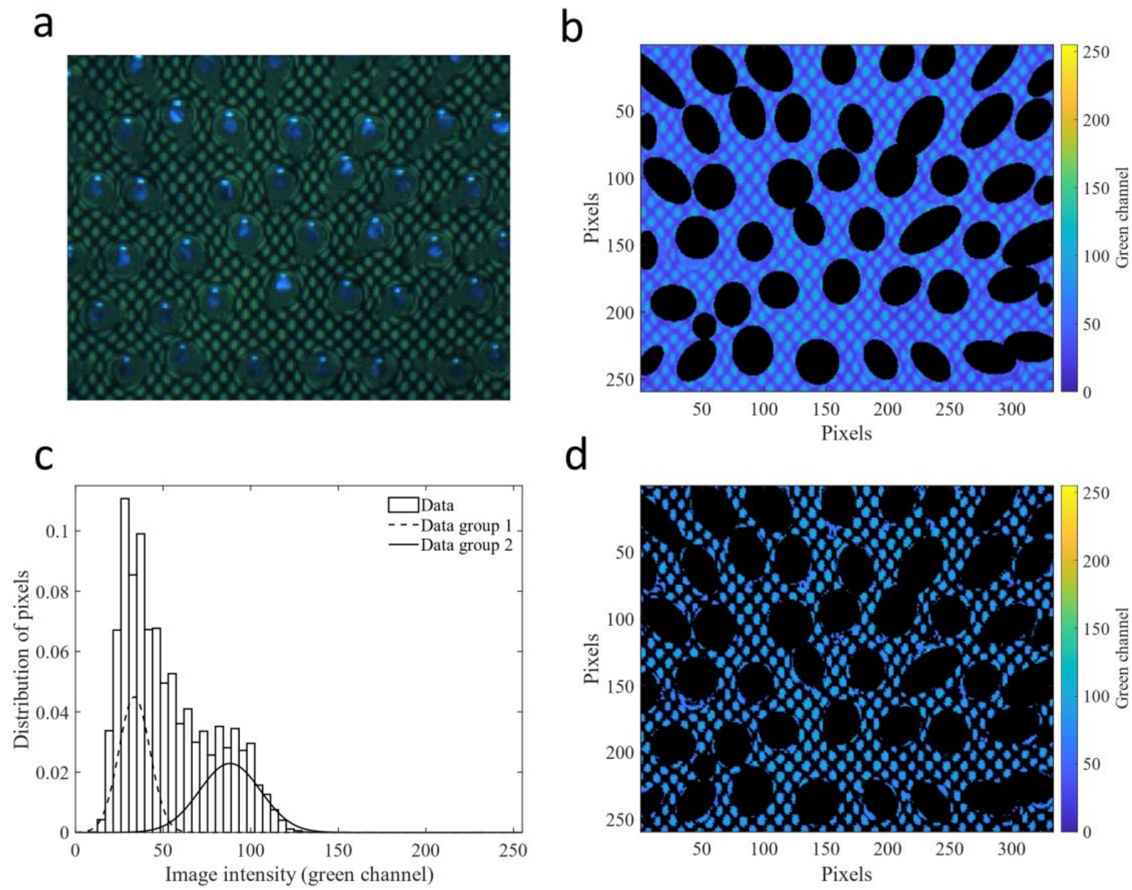

Figure S6. Image processing process. (a) Crop the original image. (b) Remove the pixels occupied by vegetation dowels. (c) Separate pixels into two groups. (d) Locate the pixels occupied by hydrogel beads and pore water.